

Exploring the capabilities of TM and AVIRIS sensor images for oil spill detection in marine and ocean waters

Qadir Ashournejad*, Department of RS & GIS, University of Tehran, Tehran, 19166, Iran.

Saham Mirzaei, Department of RS & GIS, University of Tehran, Tehran, 19166, Iran.

Seyyed Javad Hoseini, Department of Physical Geography, University of Tehran, Tehran, 19166, Iran.

Suggested Citation:

Ashournejad, Q., Mirzaei, S. & Hoseini, S. J. (2017). Exploring the capabilities of TM and AVIRIS sensor images for oil spill detection in marine and ocean waters. *World Journal of Environmental Research*. 7(2), 72-87.

Received June 17, 2017; revised September 28, 2017; accepted December 28, 2017.

Selection and peer review under responsibility of Prof. Dr. Haluk Soran, Near East University, Cyprus.

© 2017 SciencePark Research, Organization & Counseling. All rights reserved.

Abstract

Oil spills are major water polluting sources. Due to its devastating effects on the sea and ocean ecosystem, detecting oil pollution in the shortest time and with the highest confidence level is necessary. Remote sensing being a suitable option, the capability of Landsat multispectral data and airborne hyper-spectral data from the AVIRIS sensor was investigated for study of the 2001 oil spill in the Gulf of Mexico. In this study, a part of the 2001 oil spill data was processed in terms of cloud spots, bad pixel and atmospheric correction. The pixel purity index was used to extract the end-members of water and oil spill and the linear spectral unmixing method was used for mapping of water from oil spills. The results show that the AVIRIS image is able to detect the type and thicknesses of oil spill, due to its ability to cover the diagnostic spectral signature of oil.

Keywords: Monitoring, oil spill, remote sensing, Landsat, AVIRIS.

* ADDRESS FOR CORRESPONDENCE: **Qadir Ashournejad**, Department of RS & GIS, University of Tehran, 16166, Tehran, Iran.
E-mail address: ashournejad@ut.ac.ir / Tel.: +98 21 61111

1. Introduction

The importance of the seas and oceans in transport, fisheries, energy, vast mineral resources and their contribution to maintaining the ecological balance is crucial and significant (Lotfi, Baghayi, Mousavi & Khayambashi, 2011). Oceans and seas cover more than 360 million sq km, about 71% of the earth's surface, and being the most important constituent of the hydrosphere, they have an undeniable role in human life. Therefore, human life is directly or indirectly dependent on seas and oceans. In recent years, exploitation of the seas and oceans has been widespread and has led to contamination of water bodies and coastlines. Oil is considered as one of the main pollutants in these environments (Rangzan & Abidavi, 2016). Actually, oil contamination is an inevitable consequence of the anomalous extension of technology (Kheirabadi & Mohammadi, 2004). The oil released from tankers, ships and oil pipelines has been an issue in recent years that is widely taking place (Goldaraq & Salehi, 2011), and due to increased oil production and the transportation industry, this type of pollution is rapidly growing (Shahini et al., 2012). In this respect, attention to environmental impact, which is one of the most important elements of sustainable development, is crucial in implementation of oil projects (Ahmadi & Ahmadi, 2014).

One of the causes of oil pollution of the oceans is tanker accidents, the largest of which occurred in 1967 in British waters. In 1975 in South Carolina, about a thousand gallons of oil effused from a petroleum tank into the sea. Also in 1991, release of petroleum in the Persian Gulf caused destruction of aquatic plants and of coastal ecosystems. Every year, 48% of the pollution in seas and oceans is related to fuel, and 29% is related to petroleum, with tanker accidents causing only 5% of contaminants entering the seas and oceans. In addition, approximately 45% of the oil contamination occurs during ship discharge. As regards repeated leaks, it can be stated that such leaks can be a much more serious threat to the environment and marine ecosystems than accidents of ships and oil tankers (Rangzan & Abidavi, 2016). In order to effectively protect the ecosystem of seas and oceans, rapid and accurate determination of oil-contaminated areas is required and necessary (Kheirabadi & Mohammadi, 2004). Remote sensing is capable of data acquisition in different parts of the electromagnetic spectrum and in short timescales, and vast zonal horizon, making it a suitable option for detection and immediate monitoring of oil spills (Matakan, Hajab & Azarakhsh, 2014). This reveals that remote sensing through collecting appropriate data sources generally plays a significant role in management of different sources in terms of controlling and monitoring of environmental pollution (Rangzan & Abidavi, 2016).

2. Remote Sensing to Detect Oil Pollution

Remote sensing tools that are used for detection of oil spills include photos and infrared videos, thermal infrared imagery, airborne fluorescence laser, airborne and space optical sensors and airborne and space SAR (Matakan et al., 2014).

The British petroleum oil spill was one of the worst environmental disasters and the largest oil spill in the history of America that occurred was in the Gulf of Mexico (Khanna et al., 2013). Regarding the investigation of oil spill by remote sensing, many studies have been carried out. A comprehensive research study on this issue is the study by Leifer, Lehr, Simecek-Beatty, Bradley, and Clark (2012). They studied the data AVIRIS, Moderate Resolution Imaging Spectroradiometer (MODIS), SAR and CALIPSO on the oil spills (Leifer, Lehr, Simecek-Beatty, Bradley & Clark, 2012). In several studies, Fingas and Broen as well investigated oil spills using remote sensing (Fingas, 1996, 2011; Fingas & Broen, 1997, 2002, 2011, 2014). Clark et al. (2010) explored the capabilities of AVIRIS airborne hyper-spectral sensor in detecting oil spills with a focus on the Gulf of Mexico oil spill and examined the spectral behaviour of oil spills of varying thicknesses (Figure 1).

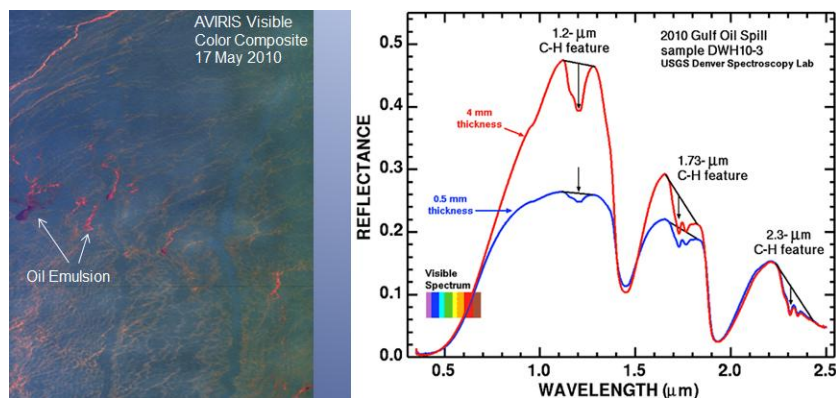


Figure 1. The spectral behaviour of oil spills of varying thicknesses in hyper-spectral image sensor AVIRIS (Clark et al., 2010)

Kokaly, Couvillion, Holloway, Roberts, and Ustin (2013) used airborne hyper-spectral sensor data AVIRIS during and after leakage of an oil spill to map the distribution of affected swamp plants. They compared AVIRIS data through absorption phenomena at approximate ranges of 1.7 and 2.3 μm with the reference spectrum of oil-polluted swamps and the results demonstrate the effectiveness and efficiency of hyper-spectral data with high spectral power in assessment of the ecosystem disruption and its response (Kokaly, Couvillion, Holloway, Roberts & Ustin, 2013).

Taravat and Del Frate (2012) with the band ratio algorithms and artificial neural network showed the capability of the Landsat ETM+ images in order to identify oil spill pollution. The results indicate the potential of these data for detecting the oil spills (Taravat & Del Frate, 2012). Zhao, Temimi, Ghedira, and Hu (2014) examined the visible and infrared spectral signs of oil spills observed in the shallow beaches of the Persian Gulf using MODIS, Medium Resolution Imaging Spectrometer and Landsat images. They suggest a warning system and decision support system based on interaction between remote sensing data and hydrodynamic models to respond to oil pollution (Zhao, Temimi, Ghedira & Hu, 2014).

Al-Hinai, Khan, Dabbagh, and Bader (1993) also examined the 1991 Persian Gulf oil spills using the Landsat TM image. Kolokoussis and Karathanassi (2013) examined the ability of multi-spectral data for detecting oil spills and provided an object-based approach using the data. Their method had good results and used the data from IKONOS, QuickBird, RapidEye, and WorldView2 as well as Landsat TM data (Kolokoussis & Karathanassi, 2013).

The aim of this study is to identify and evaluate the ability of oil spills detection by the acquired data from Landsat multispectral, and to compare them with airborne hyper-spectral data AVIRIS. For this purpose, the study was conducted on the Gulf of Mexico oil spill in 2010.

3. Research Method

In this study we used AVIRIS hyper-spectral images taken on 19 May 2010 for the Gulf of Mexico along with multispectral Landsat TM data on 25 May 2010 (Figure 2).

The hyper-spectral imagery (Landsat AVIRIS) is taken in the spectral range of 0.4 to 2.5 μm by 224 bands and spatial resolution of 12.1 m and radiometric resolution of 16 bits at a height of 13.7 km (45,000 feet).

Also, in this research, TM images were used with details provided in Table 1. Landsat satellite series provide unique data source for mapping, monitoring and management of land resources. The value of the Landsat data includes long-term duplicate cover and relatively appropriate spatial resolution.

Table 1. Properties of the data used

Sensor	Spatial resolution	Radiometric resolution	Row number	Pass number	Band number	Imaging date
AVIRIS	12.1 m	16 bit	-	-	1-224	2010.05.19
TM	30 m	8 bit	40	21	1-7	2010.05.25

Given the importance of pre-processing operations on remote sensing data, first the data were controlled in terms of the cloud spots in the image, signal-to-noise ratio, etc. Next, the pixel purity index (PPI) and linear spectral unmixing (LSU) algorithm were used to extract the end-members of water and oil spill and to map the oil spills. In this study, Environment for Visualizing Image and ERDAS software were used for pre-processing and processing of data.

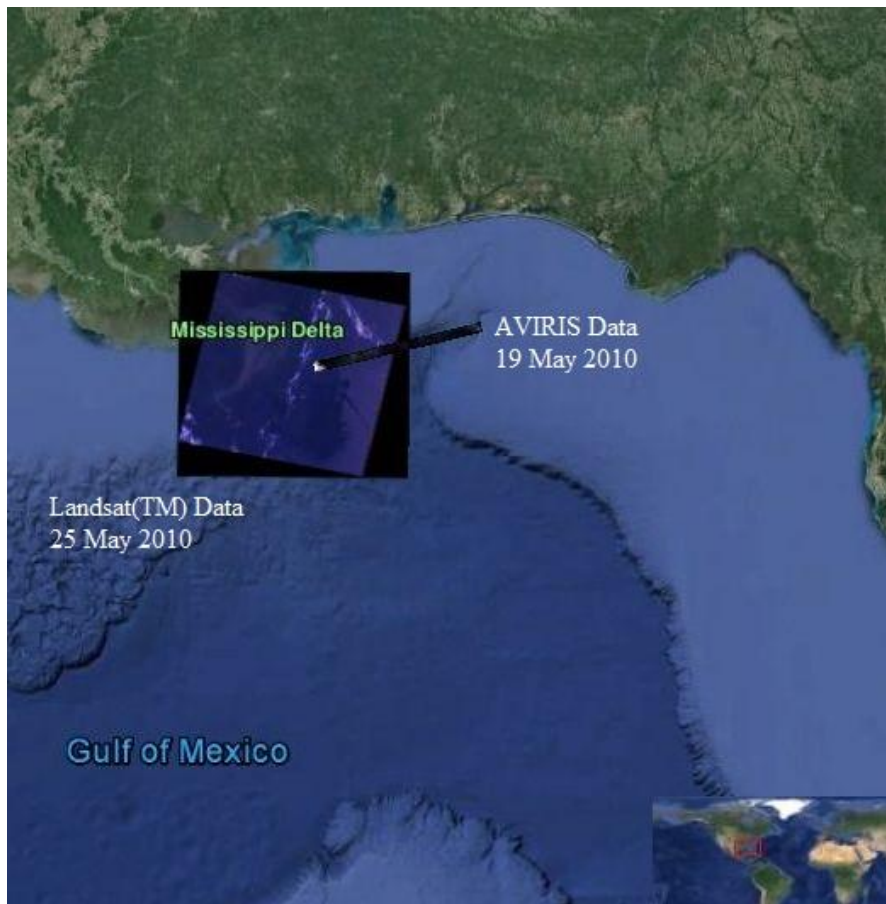


Figure 2. AVIRIS and Landsat imaging range in the Gulf of Mexico

4. Processing and Processing of Landsat Image

4.1. First step: Identifying defective pixels and investigating noise of bands

4.1.1. Identifying and removing bad pixels

First, a part of the image was selected from the whole image to be checked for oil spills (Figure 3). According to the image metadata, parts of the image that are cloudy should be identified and excluded from the calculations before pre-processing. This is performed by determination of

thresholds on the bands distinguishing cloud from other phenomena. By investigating the spectral behaviour of the cloud (Figure 4), high reflectance in bands 1, 3 and 5 observed that among these, oil spills also have a high reflection on the band 5 (Figure 4). As a result, we used band 1 with digital values (DN) threshold above 100 for separation of cloud. By rechecking the image, we observed non-complete removal of clouds; therefore, by changing the threshold from 100 to 90 (90–255), the clouds were completely removed from the image.

Identifying some of the bad pixels is not possible while there is cloud. Therefore, the signal-to-noise analysis, statistical filtering (for removing the periodic noise and replace bad line to detect and correct bad pixels according to neighbours) were done on the images.

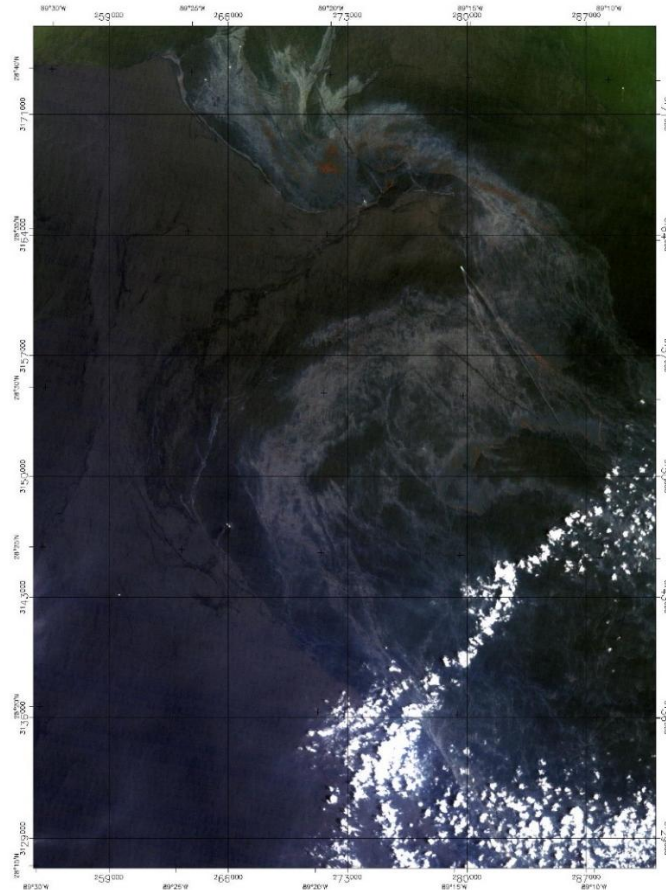


Figure 3. The study area identifying oil spills on the Landsat TM image

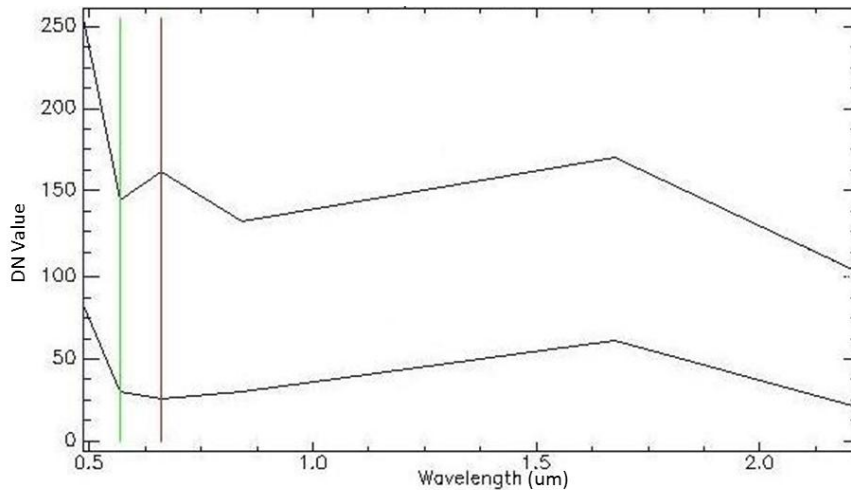


Figure 4. Spectral behaviour of the cloud and oil spill on the Landsat TM image

4.2. Step two: Applying gain and offset on the bands

First of all, in order to correct the data, DN were converted to spectral radiance using sensor calibration coefficients (gain and offset). DN was recorded by the sensors of a given phenomenon, influenced by the viewing angle, position and angle of the sun, weather conditions, time, etc. Therefore, it is very useful in satellite image processing for various quantitative and qualitative applications where DN are converted to spectral reflectance units, and therefore, true reflection of the phenomenon were used in the analysis. The advantage of this conversion is the ability to compare different levels of spectral reflectance of phenomenon between temporal images, as well as creation and application of spectral library of terrestrial phenomena and true reflection of the phenomenon (Rudgarmy, Khorasani, Monavari & Noori, 2010).

4.3. Step three: Atmospheric correction

Log residuals method is used to perform atmospheric corrections and converting radiance to reflectance (Figure 5). In this method the statistical data of the images were used to calibrate and the radiance data were normalised towards the spatial geometric mean. The topographic effects are removed using the spectral geometric mean logarithm (average of all the bands for a pixel) and the effects of solar radiation, atmospheric transmittance and machine error are deleted using the spatial geometric mean (average of all pixels for each band) (Namin, Aslani & Bahroudi, 2011).

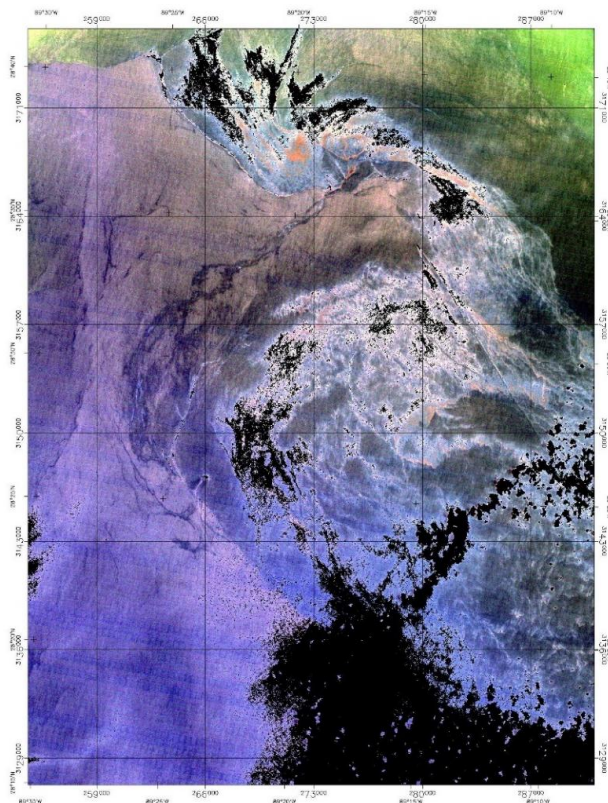


Figure 5. Atmospheric corrected image using log residuals algorithm on the Landsat TM image

4.4. Step four: Extraction of oil spills

4.4.1. LSU analysis, end-member selection and extraction

In this study, in order to extract the end-members of water and oil spills, the PPI was used and the algorithm was repeated through trial and error 10,000 times. The higher pixel value represents greater spectral purity. The PPI algorithm pixels in the study area are evaluated only in terms of spectral purity, and not spectrum type. Reflection of the pure pixels is shown in Figure 6. Then the end-member was extracted from the previous step with the help of LSU algorithms to separate water from oil spills (Figure 7). In Figure 6, the white colour represents bad pixels that were excluded from the first stage. Blue represents water and red shows oil spills with dark spots; the higher concentration is shown in darker tones than the spots with lower concentrations.

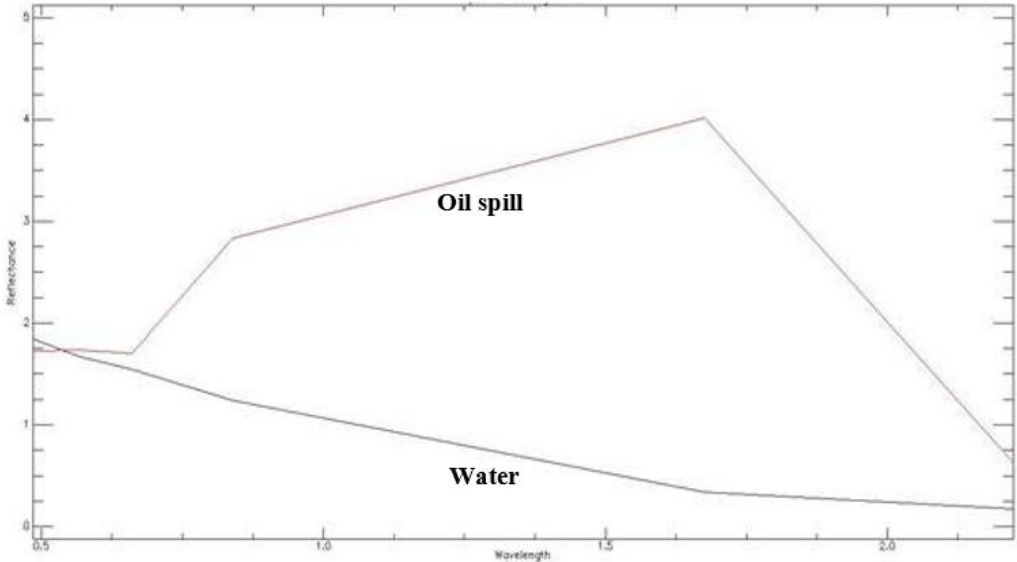


Figure 6. End-member of the water and oil spill from PPI on the Landsat TM image

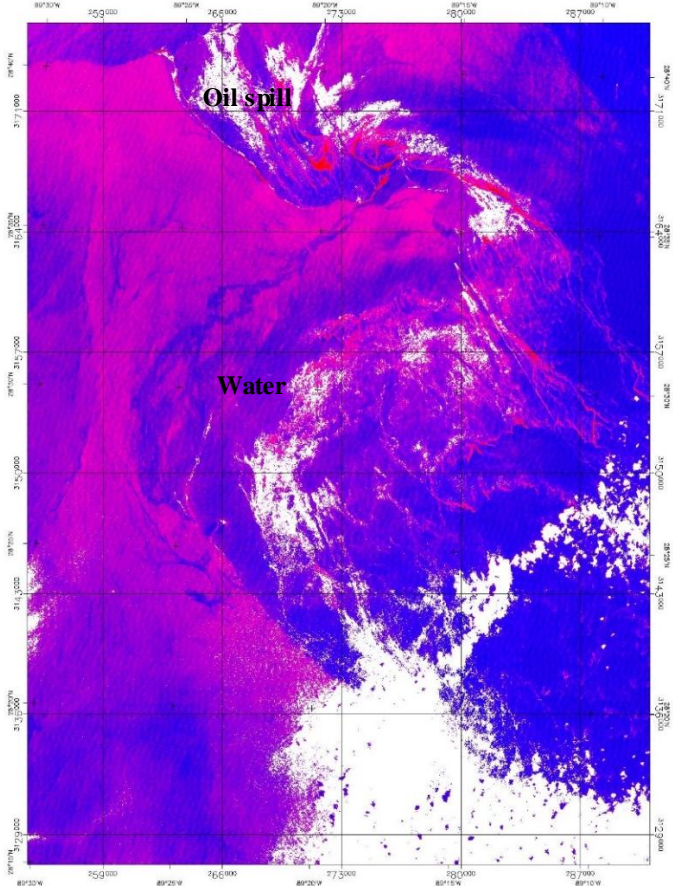


Figure 7. Unmixing the water from oil spills with LSU algorithms on the TM Landsat image

5. Pre-processing and Processing AVIRIS Data

5.1. First step: Identifying defective pixels and investigating noise of bands

5.1.1. Identifying and removing bad pixels

Regarding the AVIRIS data, part of the image was separated to investigate oil (Figure 8). According to the image metadata, 70% of the image is usable (clear). Cloud spots are also seen in the study area that should be identified and before entering the pre-processing stage excluded from the calculation process. This was performed by determination of thresholds on the bands distinguishing cloud from other phenomena. By investigating the spectral behaviour of clouds and other phenomena on the image, band 20 was selected (Figure 9).

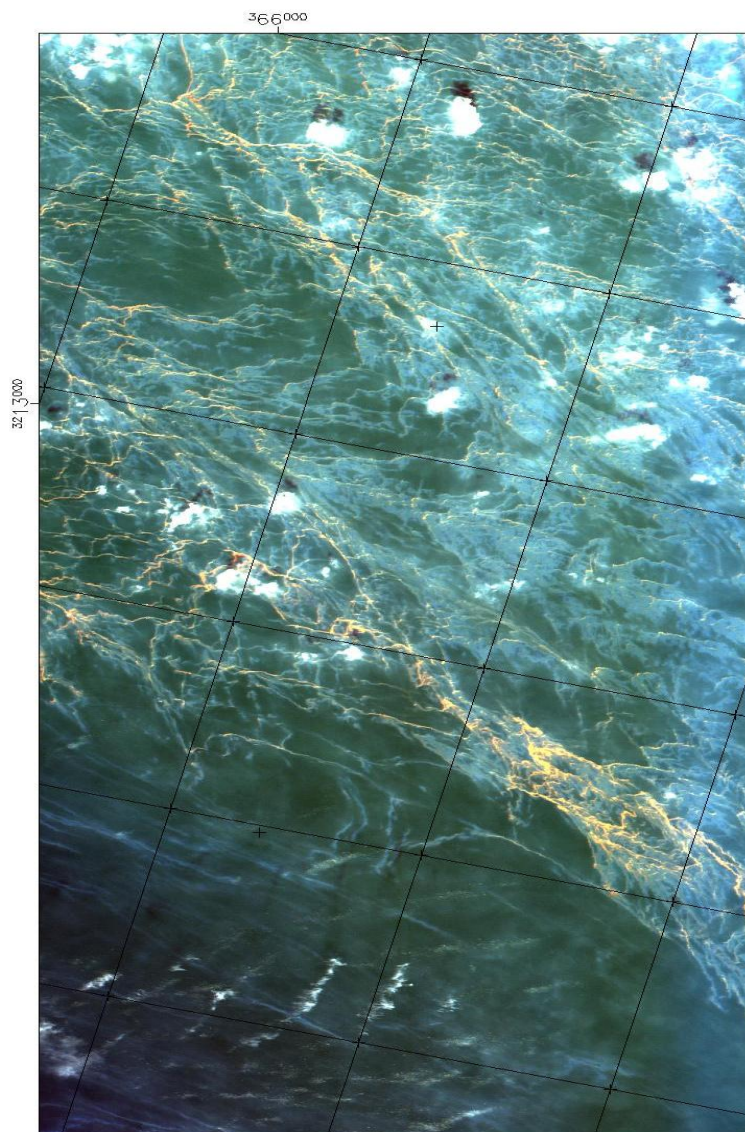


Figure 8. The study area identifying oil spills on the hyper-spectral image AVIRIS

Complete elimination of cloud using band 20 was not possible because of the possibility of removing oil spills. As a result, for complete removal of the cloud the image band 10 (the distinguishing cloud and water) was used (Figure 10).

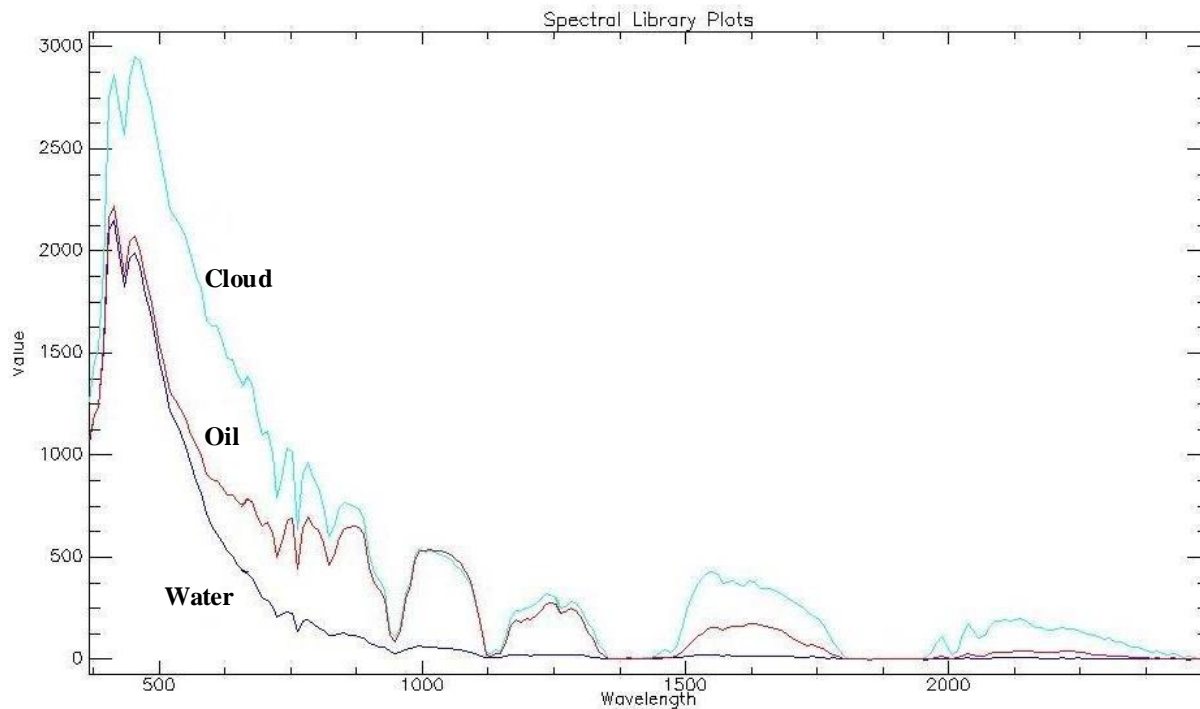


Figure 9. Spectral behaviour of cloud, water and oil spill on hyper-spectral image AVIRIS

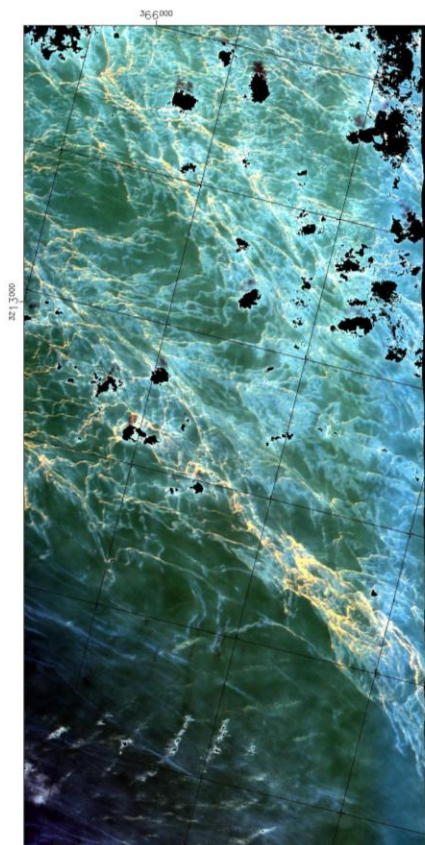


Figure 10. Removing the cloud from the study area on hyper-spectral image AVIRIS

5.1.2. Signal-to-noise control

Identifying some of the defective pixels is not possible while there is cloud and therefore the signal-to-noise analysis must be carried out. This is due to achieving more accurate results at the next stages. Based on the obtained results, due to low signal to noise, bands 39–41, 44 and 45, 49–52 and 61–65 were removed from the dataset. Also, statistical filtering is possible using the tools of statistical filter, periodic noise removal and replacing bad line in ERDAS software to detect and correct defective pixels according to neighbours, periodic noise correction and remaining or bad lines. The used image was controlled in terms of the above errors.

5.2. Step two: Applying gain and offset on the bands

At this stage, the Landsat data to convert digital values to spectral radiation sensor calibration coefficients (gain and offset) were used. The possibility of comparing different values of the phenomenon's spectral reflectance between temporal images and creation and use of spectral library of terrestrial phenomena and true reflection of the phenomenon are advantages of this conversion (Rudgarmy et al., 2010).

5.3. Step three: Atmospheric correction

For radiometric and atmospheric corrections, the Landsat data log residuals method is used. In this method, the statistical data of the images are used to calibrate. Removing the topographic effects and

the effects of solar radiation, atmospheric transmittance and machine error are also among the features of this method (Namin et al., 2011).

5.4. Step four: Extraction of oil spills

5.4.1. LSU analysis, end-member selection and extraction

For end-member extraction of water and oil spills on the AVIRIS data, PPI was also used. After applying the MNF on the images, 20 eigenvalues were selected. Pure pixel selection algorithm through trial and error was 10,000 times (Figure 11).

Then end-member extracted from the previous step with the help of LSU algorithm was used to separate water from oil spills (Figure 12). In the figure, white are bad pixels that had been excluded from the first stage. Blue represents water and the red shows oil spills with dark spots with a higher concentration shown in darker tones than the spots with lower concentrations.

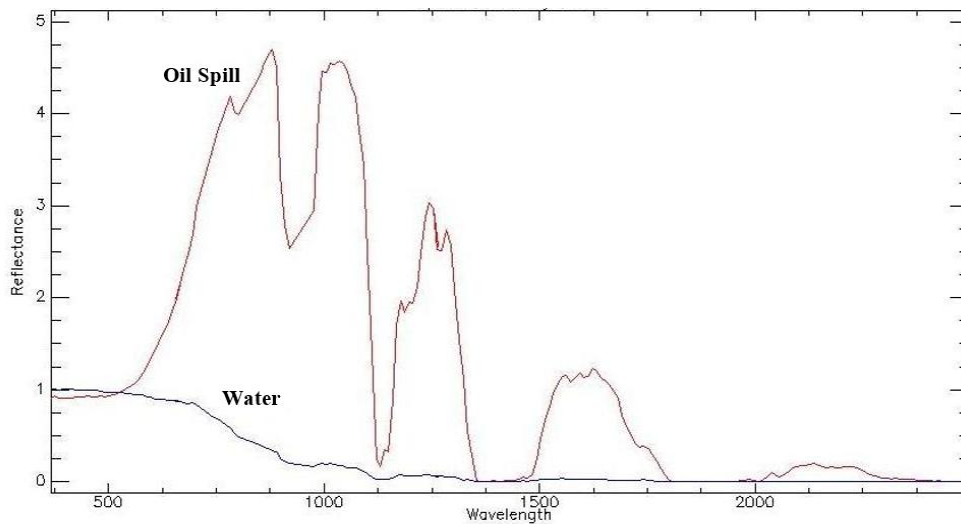


Figure 11. End-member of the water and oil spill from PPI on the hyper-spectral image AVIRIS

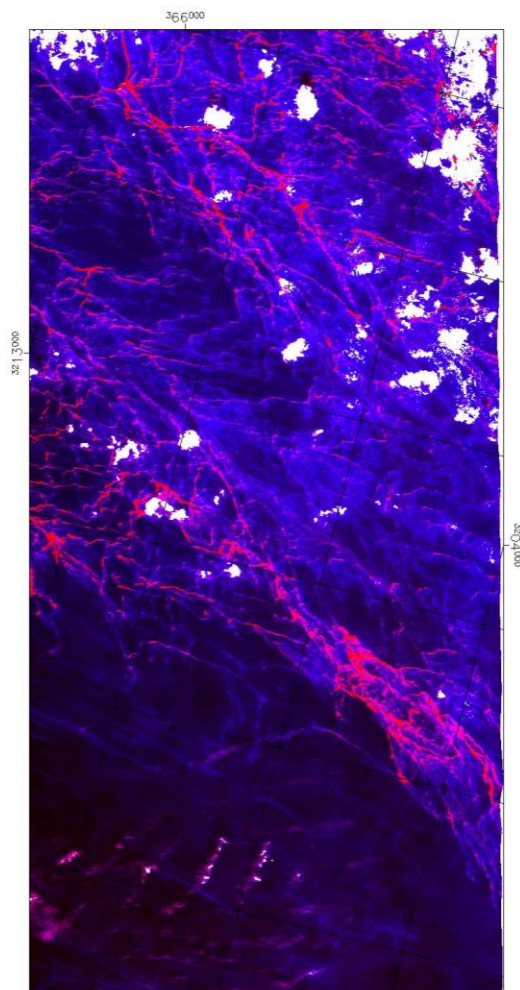


Figure 12. Unmixing the water from oil spills with LSU algorithm on the hyper-spectral AVIRIS image

6. Spectral Behaviour of Oil Spill on the Landsat Multispectral (Landsat TM) and Hyper-spectral AVIRIS Images

By overlaying the spectral behaviour of the oil spill extracted on the two Landsat and AVIRIS images (Figure 13), it is possible to identify the phenomena of absorption for the extraction of oil spills from the image as well as providing band ratios for the production of colour combinations to oil spills detection against water.

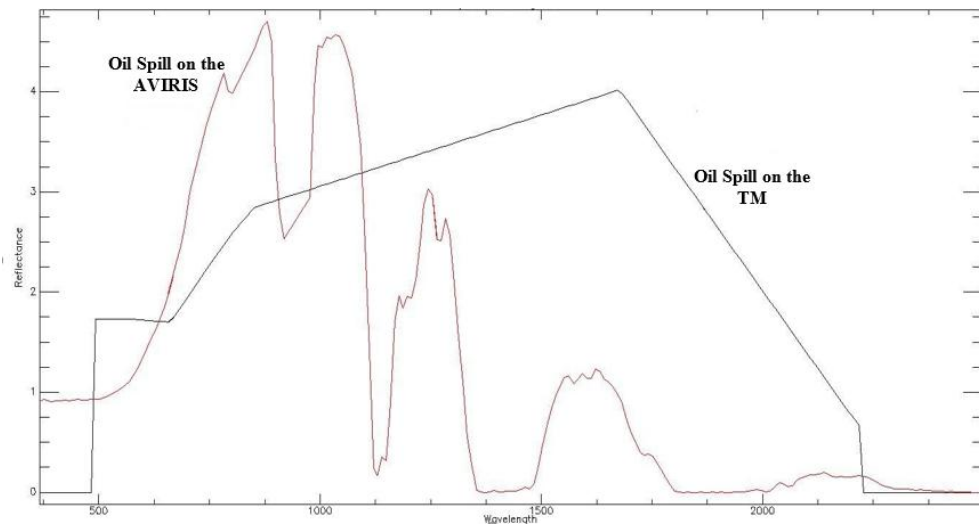


Figure 13. End-members of the oil spill from PPI on the TM Landsat and hyper-spectral image AVIRIS

According to the spectral behaviour curve of the extracted oil spill for water detection in hyper-spectral Images, AVIRIS can be used in the following proportions (Clark et al., 2010): ND1, ND2 and ND3 can be used in a colour combination of red, green and blue, respectively, as

$$ND1 = (R1_a - R1_b) / (R1_a + R1_b)$$

$$ND2 = (R2_a - R2_b) / (R2_a + R2_b)$$

$$ND3 = (R3_a - R3_b) / (R3_a + R3_b)$$

Table 2. Band numbers and spectral ranges in band ratios of the sensor AVIRIS

Normalised difference term	AVIRIS 2010 channels	Wavelengths of channels (micrometers)
R1 _a	47, 48, 49	0.793, 0.802, 0.812
R1 _b	23, 24, 25	0.580, 0.589, 0.599
R2 _a	75, 76, 77	1.063, 1.073, 1.082
R2 _b	67, 68, 69	0.986, 0.996, 1.006
R3 _a	144, 145, 146	1.722, 1.732, 1.742
R3 _b	135, 136, 137	1.632, 1.642, 1.652

According to the spectral behaviour curve of the extracted oil spill for water detection in Landsat hyper-spectral images, the following proportions can be used as in (Taravat & Del Frate, 2012). RS1, RS2 and RS3 can be used in a colour combination of red, green and blue, respectively, as

$$RS1 = (B4 / B2) / B1$$

$$RS2 = (B3 / B2) / B1$$

$$RS3 = (B3 / B2) / B1$$

In addition, this absorption phenomenon of C-H that is observed in the range of 1.2, 1.73 and 2.3 μm in experimental conditions, also revealed in the spectra of remote sensing with different intensities.

7. Discussion and Conclusion

Comparing multispectral data with hyper-spectral data may not be logical due to the different nature of the two sets of data. But the results indicate that both sets of data are capable of detecting oil spills. Due to the nature of hyper-spectral data, the difference is that AVIRIS is also able to determine the type of oil (petroleum and oil) and the thickness of the oil spill due to covering the diagnostic spectral signature of oil. Achieving these will need precise pre-processing and processing on the data using secondary data (atmospheric data, field data, etc.). However, long-term repeated coverage, easy access and relatively good spatial resolution of Landsat data compared with that of AVIRIS airborne hyper-spectral data should not be ignored. Accessibility of the airborne hyper-spectral data is usually associated with significant cost and the data are prepared in accordance with user customisation and therefore is difficult to be accessed.

References

- Ahmadi, P., & Ahmadi, G. H. (2014). *Remote sensing and prevention of environmental pollution at oil refineries in Iran*. The Second International Conference on Environmental Hazards, University of Kharazmi, Tehran, Iran.
- Al-Hinai, K. G., Khan, M. A., Dabbagh, A. E., & Bader, T. A. (1993). Analysis of landsat thematic mapper data for mapping oil slick concentrations Arabian Gulf oil spill 1991. *Arabian Journal for Science and Engineering*, 18(2), 85–93.
- Clark, R. N., Swayze, G. A., & Leifer, I. (2010). *A method for quantitative mapping of thick oil spills using imaging spectroscopy*. U.S.: Geological Survey Open-File Report Number 2010–1167.
- Fingas, M. (1996). The evaporation of oil spills: Prediction of equations using distillation data. *Spill Science and Technology Bulletin*, 3, 191–192.
- Fingas, M. (2011). An overview of in-situ burning. In *Oil spill science and technology* (pp. 737–903). Boston, MA: Gulf Professional.
- Fingas, M. F., & Brown, C. E. (1997). Review of oil spill remote sensing. *Spill Science and Technology Bulletin*, 4, 199–208.
- Fingas, M. F., & Brown, C. E. (2014). Review of oil spill remote sensing. *Marine Pollution Bulletin*, 83, 9–23.
- Fingas, M., & Brown, C. (2002). Review of oil spill remote sensors. *7th International Conference on Remote Sensing for Marine and Coastal Environments*, ERIM International, Miami, FL.
- Fingas, M., & Brown, C. E. (2011). Oil spill remote sensing: a review. In *Oil spill science and technology* (pp. 111–169). Boston, MA: Gulf Professional.
- Goldaraq, Y. J., & Saheli, M. R. (2011). Investigating the methods of detection of oil spills in seas and oceans through satellite imagery, US: Geomatics 2011, National Mapping Survey.
- Khanna, S., Santos, M. J., Ustin, S. L., Koltunov, A., Kokaly, R. F., & Roberts, D. A. (2013). Detection of salt marsh vegetation stress and recovery after the deepwater horizon oil spill in Barataria Bay, Gulf of Mexico using AVIRIS data. *Plos One*, 8(11), 1–13.
- Kheirabadi, S. M., & Mohammadi, A. A. (2004). *Evaluating of classification algorithms based on spectral angle and library in detection of oil spills on the Persian Gulf on AVHRR images, Geomatics 2004*. Tehran: national mapping survey.
- Kokaly, R. F., Couvillion, B. R., Holloway, J. M., Roberts, D. A., & Ustin, S. L. (2013). Spectroscopic remote sensing of the distribution and persistence of oil from the deepwater horizon spill in Barataria Bay marshes. *Remote Sensing of Environment*, 129, 210–230.
- Kolokoussis, P., & Karathanassi, V. (2013). Detection of oil spills and underwater natural oil outflow using multispectral satellite imagery. *International Journal of Remote Sensing Applications*, 3, 145–154.
- Leifer, I., Lehr, W. J., Simecek-Beatty, D., Bradley, E., & Clark, R. (2012). State of the art satellite and airborne marine oil spill remote sensing: application to the BP deepwater horizon oil spill. *Remote Sensing of Environment*, 124, 185–209.
- Lotfi, H., Baghayi, H., Mousavi, S. R., & Khayambashi, S. (2011). Persian gulf environment and its protection. *Human Geography*, 1, 1–9.

Ashournejad, Q., Mirzaei, S. & Hoseini, S. J. (2017). Exploring the capabilities of TM and AVIRIS sensor images for oil spill detection in marine and ocean waters. *World Journal of Environmental Research*, 7(2), 72-87.

Matakan, A. A., Hajab, M., & Azarakhsh, Z. (2014). *Introduction and evaluation of the methods of detecting oil spills on SAR images* (Twentieth Geomatics 2014, National Mapping Survey).

Matakan, A. A., Hajab, M., & Azarakhsh, Z. (2015a). Evaluating capability of features analysis based at the discovery of sea's oil pollution using SAR polarimeter data. *Radar*, 2(3), 13–24.

Matakan, A. A., Hajab, M., & Azarakhsh, Z. (2015b). Investigating application of remote sensing to detecting oil pollution in the sea. *Environmental Sciences*, 12(1), 10–11.

Matakan, A. A., Kazemi, A., Gili, M. R., & Ashorlu, D. (2009). Investigating the spatial distribution of cadmium and determining vegetation at risk in Isfahan in central Iran using GIS and RS. *Environmental Sciences*, 6(2), 65–76.

Rangzan, K., & Abidavi, Z. (2016). *Monitoring of oil pollution of the seas and oceans using remote sensing technology*. International Conference on Science, Environmental Engineering and Technology.

Rudgarmy, P., Khorasani, N., Monavari, S. M., & Noori, J. (2010). Forecasting environmental effects of development using satellite imagery and remote sensing techniques. *Environmental Science and Technology*, 11(1), 2-11.

Saghafi Far, H., & Chitsaz, M. H. (2006). *Detection of oil spills on the sea surface by LIDAR*. Center for Atmospheric and Oceanic Sciences, The Sixth Congress of Marine Science and Technology, Tehran, Iran.

Taravat, A., & Del Frate, F. (2012). Development of band ratioing algorithms and neural networks to detection of oil spills using landsat ETM+ data. *EURASIP Journal on Advances in Signal Processing*, 107, 1–8.

Zhao, J., Temimi, M., Ghedira, M., & Hu, C. (2014). Exploring the potential of optical remote sensing for oil spill detection in shallow coastal waters—a case study in the Arabian Gulf. *Optics Express*, 22, 13755–13772.